ACS APPLIED MATERIALS & INTERFACES

Research Article

www.acsami.org

# Synergistic Metal–Metal Oxide Nanoparticles Supported Electrocatalytic Graphene for Improved Photoelectrochemical Glucose Oxidation

Anitha Devadoss,[†,‡,§] P. Sudhagar,[†,§,∥] Santanu Das,[⊥] Sang Yun Lee,[#] C. Terashima,[∥] K. Nakata, A. Fujishima,[∥] Wonbong Choi,*[,⊥] Yong Soo Kang,[§] and Ungyu Paik*[,‡,§]

[‡]Department of Materials Science Engineering, [§]WCU Department of Energy Engineering, Hanyang University, Seoul 133-791, Korea

[⊥]Department of Materials Science and Engineering, University of North Texas, Denton, Texas, 76207, United States

[#]Institute of Nano Science and Technology, Hanyang University, Seoul 133-791, Korea

[∥]Photocatalysis International Research Center, Tokyo University of Science, 2641 Yamazaki, Noda, Chiba 278-8510, Japan

Supporting Information

**ABSTRACT:** We report the fabrication of graphene–$WO_3$–Au hybrid membranes and evaluate their photocatalytic activity towards glucose oxidase mediated enzymatic glucose oxidation. The dual-functionality of gold nanoparticles in the reinforcement of visible light activity of graphene–$WO_3$ membranes and improving the catalytic activity of immobilized enzymes for unique photoelectrochemical sensing application is demonstrated. This work provides new insights into the fabrication of light-sensitive hybrid materials and facilitates their application in future.

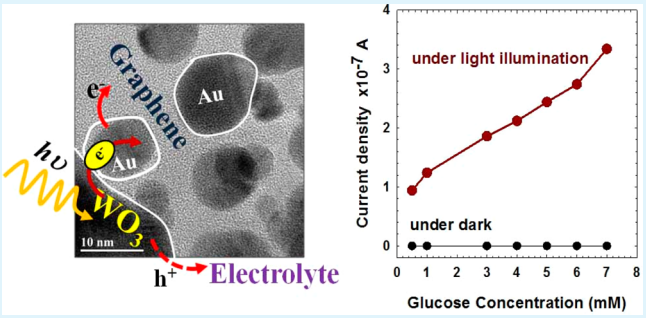


**KEYWORDS:** *graphene, $WO_3$, Au nanoparticles, photoelectrochemical sensing, glucose*

## 1. INTRODUCTION

For the purpose of effectively utilizing the solar light, significant efforts have been focussed on exploring new photoactive materials for catalytic applications including solar fuels, solar cells, sensors, photocatalytic (PC) dye decolourization etc.[1−4] In particular, photoelectrochemical (PEC) sensing has become a new and promising analytical tool for the detection of biomolecules.[5,6] PEC sensing is a low-cost detection method, which involves the electron transfer reaction among the photoactive material, analyte, and the electrode upon light irradiation. Such sensors exhibit high sensitivity and low background due to the separation between the excitation source[7] and the detection signal (photocurrent). However, the performance and efficiency of PEC sensors primarily depends on the PC ability of the active materials. In recent years, PEC detection of biomolecules such as DNA, glucose, NADH etc. are successfully demonstrated using $TiO_2$ nanomaterials.[8−11] In spite of the successes, the direct utilization of pure $TiO_2$ nanomaterials for biosensing applications is limited because of the wide band gap nature of $TiO_2$,[3] which absorbs UV light that could deactivate the biomolecules.[8,12] Thus, there exists an increased demand for the fabrication of visible light sensitive materials with excellent PC activity. On this note, tungsten oxide ($WO_3$) is gaining considerable attention in PEC based applications due to its excellent light absorption behaviour in the visible region, high chemical stability, increased photocorrosion resistivity, and excellent electron transport behavior.[13−15] However, the photo conversion efficiency, the suppression of the recombination of photo-generated electron-hole pairs as well as the effective utilization of visible light still remains challenging for $WO_3$ based PEC processes to become economically feasible. Thus, reducing the recombination rates and boosting the PC properties of $WO_3$ nanomaterials is critical for exploiting $WO_3$ as an alternative photoanodes in PEC cells.

A variety of strategies have been developed to improve the PEC performance, for example, anion doping, dye sensitization, and formation of composite semiconductors.[16−18] One potential means of reducing the charge recombination is to improve the charge separation via introducing new electron conductive channels in between the active materials.[19] In this context, graphene has been making a profound impact on the PEC applications owing to its unique 2D structure, superior chemical stability, and remarkable conducting properties.[20,21] Recent reports show that the incorporation of metal oxides ($TiO_2$, ZnO, etc) on graphene exhibits excellent PC proper-

Received: December 20, 2013
Accepted: March 9, 2014
Published: March 9, 2014


**Figure 1.** Schematic representation of (a) graphene–$WO_3$–Au triplet junction for glucose sensing, (b) energy levels at graphene–$WO_3$–Au photoelectrode under light illumination and glucose oxidation mechanism.

ties.[20,22,23] Particularly, the graphene in the composite improves the conductivity, and thereby improves the electrochemical performance. Thus, introducing 2D graphene underneath the photoactive $WO_3$ nanomaterials could be a promising approach to reducing the electron-hole recombination. It is anticipated that the graphene could act as electron conducting channels which could facilitate the electron conductivity as well as perhaps reducing the accessibility of electrons for charge recombination.[24−26] Furthermore, the field of plasmonics has expanded widely due to their excellent size- and shape-dependent optical properties. Plasmonic nanoparticles find their applications in diverse fields including sensors, surface-enhanced Raman spectroscopy, PEC systems, etc.[27−29] Recently, it has been reported that the PC properties of photoactive semiconductors can be enhanced using plasmonic nanoparticles; specifically, through supplying the hot electrons from metal to semiconductor, plasmon induced heating effect, and establishment of electromagnetic field around the nanoparticles.[29−31] Q. Xiang demonstrated that the Au nanoparticle decorated $WO_3$ nanowire showed markedly high photocatalytic sensing ($H_2$) and organic pollutant removal than pristine $WO_3$ nanorods.[32] Also, it has been reported that the supported metal particles (Pt-ITO-graphene)[33] or semiconductor particles (CoS-graphene-FTO)[34] showed remarkable stability at triplet junction. Furthermore, the unique metal–metal oxide–graphene triplet junction might enhance the catalytic activity of the electrode in biomedical applications.[26,35,36] Herein, we report the fabrication of graphene–$WO_3$ membranes with excellent photocatalytic activity and the possibility of fortification of their visible light activity using gold nanocrystals (AuNPs).

Glucose plays a vital role of a biomarker in the clinical therapy of diabetes.[37,38] As a proof-of-concept application, we demonstrate the photo-electrochemical oxidation of glucose using graphene–$WO_3$–Au hybrid membranes modified electrodes. Panels a and b in Figure 1 depict the schematic representation of mechanism of glucose oxidation at the graphene–$WO_3$–Au hybrid membrane modified with glucose oxidase (GOD) enzyme. Typically, under light irradiation, the photoactive $WO_3$ nanoparticles generate electron-hole pairs. It is realized that $WO_3$ is effective photoelectrode for water oxidation since its valence band maximum (VBM) position lies below the $H_2O/O_2$ oxidation potential (NHE ≈ 2.97 eV) at standard conditions.[39] Further these photogenerated holes were scavenged by biological analyte (acts as electron donors), resulting in the oxidation of the biomolecules through intermediate reaction through electron acceptor FAD/$FADH_2$ (Figure 1b). During this cycle the glucose is oxidized to gluconic acid at NHE approximately −0.4 V. Concurrently, on the cathode (Pt), the photogenerated electrons reduce water to form $H_2$. The generated photocurrent passing through the circuit is recorded as the sensing signal. Thus, the PEC sensor performance exclusively depends on the efficiency of photoactive materials in responding to the biomolecules of interest and transduction efficiency. Recently, we have reported that the presence of AuNPs in Nafion-gold composite nanofibers improved the catalytic activity of horseradish peroxidise (HRP) enzyme towards the oxidation of $H_2O_2$.[40] In this contribution, it is observed that the AuNPs could not only improve the catalytic activity of the enzymes in PEC systems (electron route denoted as II in Figure 1) but also promote the charge collection at $WO_3$/Graphene interfaces (electron injection denoted as I in the Figure 1) via forming the Schottky junction. A detailed exploration on the structural, optical, and PEC properties are carried out to gain some new insights into the fundamental mechanism.

## 2. EXPERIMENTAL SECTION

**2.1. Synthesis of Graphene–$WO_3$ Membrane.** Graphene was synthesized on 50 μm thick Cu foil (NIMROD HALL, USA) by the chemical vapour deposition of methane ($CH_4$) under reducing atmosphere. The substrates were cleaned using acetone, methanol, and 2-propanol consecutively in a sonicator for 15 minutes, followed by the dry nitrogen blowing for the removal of the solvent residue and dirt. The cleaned metal foils were annealed at 1000 °C for 1 h followed


dx.doi.org/10.1021/am4058925 | ACS Appl. Mater. Interfaces 2014, 6, 4864−4871

by the etching of surface oxide layer in a hot acetic acid bath at 60 °C. The annealed foil was further cleaned by the three-step solvent cleaning associated with sonication process. The cleaned metal foils were placed inside a two inch diameter quartz tube of a low pressure thermal chemical vapor deposition (LPCVD) system (ATOMATE, USA). The furnace temperature was ramped up to 1000 °C at a heating rate of 120 °C per min. The furnace atmosphere was kept inert throughout the heating process. Initially, the LPCVD furnace was kept under a constant flow of Ar atmosphere during ramping and finally, a mixture of $CH_4$:$H_2$ precursor gas (1:5) was flowed through the quartz tube for graphene growth at 1000 °C for 10 minutes. The as-grown graphene was characterized using Raman spectroscopy. The large-scale few-layer graphene (FLG) was transferred onto FTO glass substrate by a chemical transfer process as reported earlier.[41] The detailed transfer process is illustrated in Figure S1 (see the Supporting Information). $WO_3$ nanoparticles were deposited on graphene membrane using radio frequency sputtering inside of an ultra-high vacuum chamber, under 75 W power and 10 mTorr ambient pressure with the flow of Ar:$O_2$ (1:1).[5]

**2.2. Synthesis of AuNPs.** 4-Dimethylaminopyridine (DMAP) protected AuNPs were synthesized using the phase transfer procedure reported earlier.[42] Briefly, 30 $cm^3$ of a 30 mM aqueous solution of $HAuCl_4 \cdot 3H_2O$ was added to 80 $cm^3$ of 25 mM tetraoctylammonium bromide in toluene. Then, 25 $cm^3$ of 0.4 M aqueous $NaBH_4$ was added drop-wise to the mixture with stirring, causing an immediate reduction to occur. After a few hours, the two phases were separated and the toluene phase was subsequently washed with 0.1 M $H_2SO_4$, 0.1 M NaOH, and $H_2O$ (three times), and then dried over anhydrous $Na_2SO_4$. An equal volume of 0.1 M aqueous solution of DMAP was then added. The phase transfer is clearly visible as the dark pink colored solution transfers from toluene to water because of the addition of the DMAP and was complete within 1 h. The as prepared DMAP-protected AuNPs exhibit very high stability.

**2.3. Synthesis of Graphene–$WO_3$–Au Hybrid Membrane.** AuNPs were assembled on graphene–$WO_3$ membranes electrostatically. Typically, the electrodes modified with graphene–$WO_3$ membranes were immersed in the aqueous solution containing $3.3 \times 10^{-6}$ M DMAP-protected AuNPs for 1 min. The strong electrostatic attractive force existing between the positively charged AuNPs and negatively charged (because of the existence of OH groups at the surface) host surface ($WO_3$ NWs and graphene) makes it feasible for the sturdy attachment. The electrodes were washed with water to remove the weakly bounded AuNPs and dried under nitrogen.

**2.4. Characterization Techniques.** The morphology of graphene-$WO_3$ membranes and graphene–$WO_3$–Au hybrid membranes were characterized using the field emission transmission electron microscope (FE-TEM, FEI, Tecnai F20). The surface topography of graphene-$WO_3$ membrane modified electrode was investigated using atomic force microscopy (AFM), (Nanoscope, Dimension-3100 Multimode), and the AFM tip was a silicon-SPM sensor (tapping mode), thickness 4 $\mu$m, length 125 $\mu$m and width 30 $\mu$m. Raman spectroscopy was carried out in a system with a spectral resolution of 4 $cm^{-1}$ with an argon ion (Ar+) laser (Spectra Physics, model 177G02) of wavelength 514.5 nm. The Raman spectra were collected using a high-throughput holographic imaging spectrograph (model HoloSpec f/1.8i, Kaiser Optical Systems) in built with a volume transmission grating, a holographic notch filter, and a thermoelectrically cooled CCD detector (Andor Technology). The Raman-Spectra was collected at room temperature under normal atmospheric pressure for both graphene and graphene-$WO_3$ membrane as shown in Fig. 2. The electrochemical analysis was done using three electrode systems in which a modified FTO electrode was used as the working electrode, Ag/AgCl as the reference and Pt foil as the counter electrode. 0.1 M phosphate buffered saline (PBS) solution (pH 7.3) was used as the electrolyte for all electrochemical measurements. Cyclic voltammograms were recorded using the advanced potentiostat (PGSTAT-30 from Autolab) with the scanning voltage in the range of −1 to 1.5 V. The photocurrent measurements were recorded in 1 sun condition (100 mW $cm^{-2}$) with the visible light irradiation using a solar simulator with a 300 W xenon arc-lamp (Newport). The light intensity was calibrated using a silicon solar cell (PV measurements, Inc.)

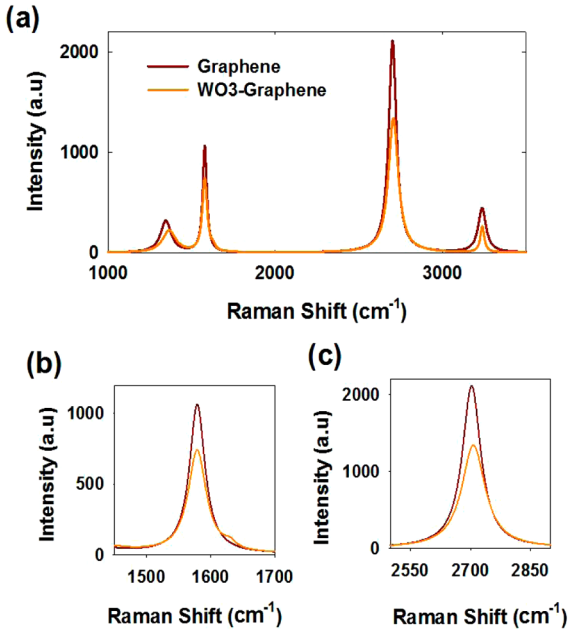


**Figure 2.** (a) Raman spectra of pristine graphene and graphene–$WO_3$ membranes; enlarged view of Raman spectra: (b) D band, (c) G band.

## 3. RESULTS AND DISCUSSION

Pristine graphene and graphene-$WO_3$ membranes on FTO are characterized using Raman spectroscopy to investigate the successful transfer of graphene membrane on FTO. Figure 2 shows the typical Raman spectra obtained for graphene and graphene-$WO_3$ membranes. The D-band and G-band in Raman spectrum of graphite symbolize the disorder band and the tangential bands respectively, whereas the symmetric 2D band illustrates the stacking order of graphene layers. It is observed that the Raman spectra of graphene exhibit characteristic D-band, G-band, and 2D band of graphene at their respective positions of ~1345, 1578, and 2702 $cm^{-1}$, as shown in Figure 2. Furthermore, the symmetric G band and 2D band positions and their corresponding band intensity ratio of $I_G/I_{2D} \approx 0.50$ clearly demonstrate the existence of few layer graphene film on FTO. The appearance of D-band in pristine graphene (PG) at 1345 $cm^{-1}$ reflects the presence of patchy graphene structure formation during the CVD process and the presence of incoherence interfaces between the graphene and the FTO.[43] A significant blue shift of ~21 $cm^{-1}$ is found for D band of graphene–$WO_3$ membrane depicting the strain induced defects in graphene–$WO_3$ structure because of the deposition of $WO_3$ nanoparticles. Interestingly, there is no peak shift found for G-band of graphene–$WO_3$ membrane (Figure 2b), which implies that the graphene underneath the $WO_3$ nanoparticles is exhibiting its inherent $sp^2$ bonded structure. On the other hand 2D peak in the Raman spectrum of graphene–$WO_3$ is shifted to higher frequency region showing the alteration in the electronic structure due to the formation of the catalytically active triple-junction at the graphene–$WO_3$ interface (Figure 2c). However, no significant differences were found in the peak intensity ratios between the G-bands and 2D band (IG/I2D of 0.5 and 0.55, respectively) for pristine graphene and graphene-$WO_3$ membrane. This corroborates the nearly unchanged graphene structure despite the $WO_3$ nanoparticles decoration.

In this context, the D-band at 1629 $cm^{-1}$ of graphene–$WO_3$ (As shown in Figure 2b) suggests the formation of dangling bonds between $WO_3$ nanoparticles and carbon atoms at the interface.[44] Furthermore, the increase in the D-band intensity as well as the appearance of D-band also manifests the prevailing heterogeneous superstructure at the interface of graphene and $WO_3$.[45] The coating of $WO_3$ on graphene surface has further ensured with ultraviolet photoelectron spectroscopy (UPS) (see the Supporting Information, Figure S2). The work function of graphene at vacuum $\Phi$ = 5.21 eV is reduced to $\Phi$ = 4.88 eV under $WO_3$ coating. This implies that the $WO_3$ is formed on the graphene matrix.

In order to map the distribution and size of $WO_3$ nanoparticles formed on graphene membrane, we probed the AFM images of graphene–$WO_3$ membranes in the tapping mode and are shown in Figure 3. The low-magnification AFM

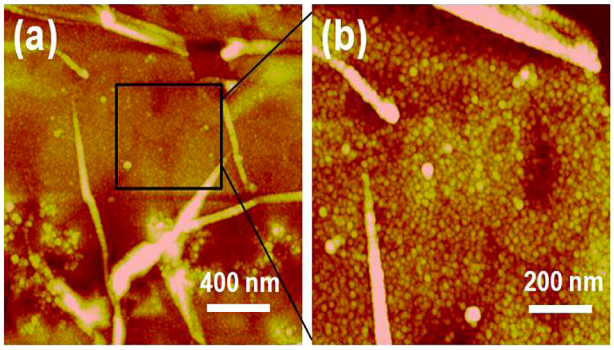


**Figure 3.** Low- and high-magnification AFM images of graphene–$WO_3$ membrane recorded in the tapping mode.

image (Figure 3a) shows that the $WO_3$ nanoparticles are well dispersed on the graphene, which is unaffected despite the transfer process. Figure 3b shows the uniform size distribution of $WO_3$ nanoparticles. The quantification of size of $WO_3$ nanoparticles was carried out using height profiles (see Figure S3 in the Supporting Information), which confirms that $WO_3$ nanoparticles with a mean diameter of about 20–30 nm were distributed uniformly on graphene. Colloidal AuNPs were prepared using the phase transfer protocol, which exhibited a high degree of monodispersity with a mean diameter of about 5 nm. Figure S4 in the Suporting Information shows the high-magnification TEM images of AuNPs and the corresponding histogram illustrating the size distribution of AuNPs. The distribution of electrostatically assembled AuNPs on graphene-$WO_3$ membranes was analysed through TEM images. Images a and b in Figure 4 show the TEM images and the inset figures show the diffraction patterns obtained for the electrodes modified with graphene and graphene–$WO_3$–Au hybrid membranes, respectively. It is observed from Figure 4a that the graphene nanosheets are well-formed and dispersed. The higher magnification images of graphene and graphene–$WO_3$–Au hybrid membrane are given in images c and d in Figure 4, respectively. The TEM images clearly confirm the existence of $WO_3$ nanoparticles and AuNPs on graphene membrane. No aggregation of AuNPs was observed in the TEM analysis. Figure S5 in the Supporting Information shows the elemental mapping of graphene–$WO_3$–Au hybrid membrane, which confirms the co-existence of each element. Moreover, the obtained diffraction patterns are also in agreement with the EDS results.

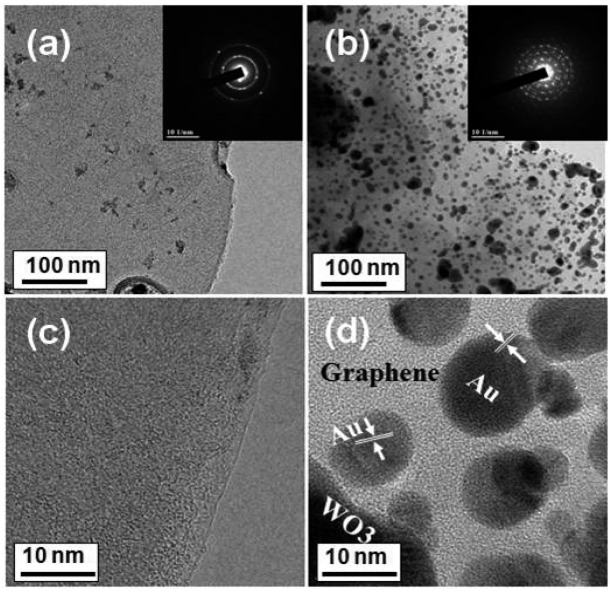


**Figure 4.** Low- and high-magnification TEM images of (a, c) graphene and (b, d) graphene–$WO_3$–Au hybrid membrane, respectively. The inset figure shows the respective diffraction patterns.

The visible light activity of the modified electrodes was analysed using UV–vis absorption measurements. Fig. 5 shows

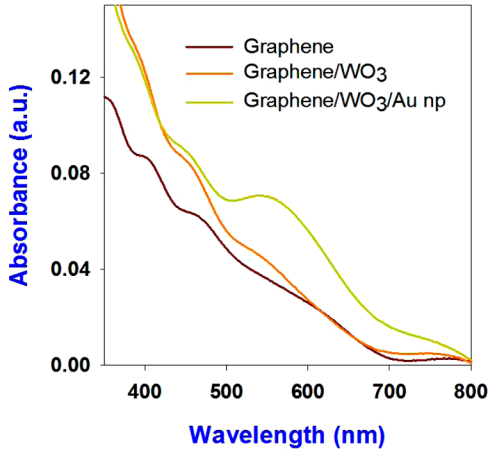


**Figure 5.** Optical absorbance of electrodes modified with graphene, graphene–$WO_3$ membrane, and graphene–$WO_3$–Au hybrid membranes.

the UV–vis absorption spectra obtained for the electrodes modified with graphene, graphene–$WO_3$ membranes, and graphene–$WO_3$–Au hybrid memebranes. The graphene–$WO_3$ membranes show an increased absorption in the visible region. As anticipated, a well-defined absorption shoulder is observed after decorating the graphene–$WO_3$ membranes with AuNPs. This is due to the strong localized surface plasmon resonance (LSPR) band of AuNPs, which is in agreement with the absorption spectrum of colloidal DMAP-protected AuNPs in water.[46] The LSPR band of nanoparticles exhibits strong dependence on the size, shape, and microenvironment of the nanoparticles. The small discrepancy observed in the absorption peak of AuNPs in Figure 5 is attributed to the changes in the microenvironment of the nanoparticles.


dx.doi.org/10.1021/am4058925 | ACS Appl. Mater. Interfaces 2014, 6, 4864–4871

The PC ability of graphene-$WO_3$ membrane and the influence of AuNPs are analysed using photocurrent studies. Fig. 6 shows the photocurrent generated at graphene−$WO_3$

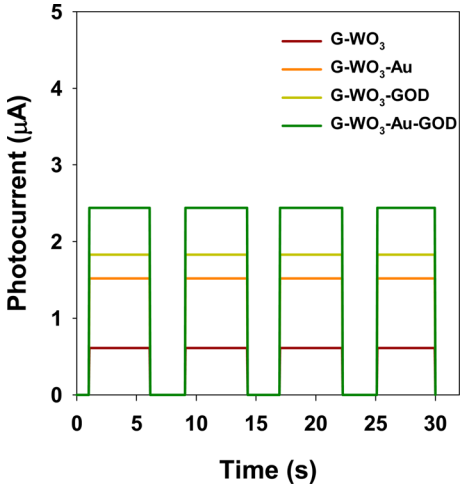


**Figure 6.** Photocurrent generated with and without AuNPs decoration at different electrodes at an applied bias of −0.4 V.

membrane before and after decorating with AuNPs in PBS buffer solution at an applied potential of -0.4 V. It is observed that the graphene−$WO_3$ membrane shows a stable photocurrent generation. Upon AuNPs decoration, the graphene−$WO_3$−Au hybrid membrane shows nearly two fold higher photocurrent generation. Figure 7a shows the cyclic voltammograms of graphene-$WO_3$ membrane and graphene-$WO_3$−Au hybrid membrane. The clear oxidation peak at 1 V corresponds to the gold oxidation. The photocurrent enhancement at Au nanoparticle decorated semiconductor/electrolyte interfaces rely on several factors: (a) hot electron injection from strong localized surface plasmon resonance from Au to semiconductor,[47,4849,] and (b) efficient charge separation at semiconductor/electrolyte interfaces through blocking the back electron transfer from semiconductor to electrolyte because of the existence of Schottky barrier at this interface.[51]

To decipher the role of Au nanoparticles in the photocurrent enhancement of graphene−$WO_3$−Au hybrid membranes, we examined the current−voltage characteristics under different light illumination conditions (Figure 7b) using high-pressure mercury arc lamp wavelength ranging from 200 to 800 nm. In the absence of UV-cut off filter, the graphene−$WO_3$−Au electrode generates photocurrent ∼0.76 mA $cm^{-2}$ at 1.0 V (vs Ag/AgCl), which was drastically reduced to ∼0.110.76 mA $cm^{-2}$ after including the 450 nm filter (ASAHI Spctra USA). Furthermore, in the case of photo illumination with 490 nm filter, photocurrent approached nearly dark current value. This confirms the negligible contribution of AuNP's plasmonic excitation towards photocurrent generation. Strikingly, the onset potential (dark) of graphene-$WO_3$−Au hybrid membranes shows a substantial negative shift of about 0.31 V (from 0.52 to 0.21 V) by photo illumination, which is attributed to the existence of effective charge separation and transportation in the electrodes. Furthermore, such negative shift corroborates that major photocurrent generation at graphene−$WO_3$−Au hybrid membranes is predominantly achieved from $WO_3$ band edge excitation (for sputtered $WO_3$ films band edge varies from 2.75 to 3.2 eV based on the oxygen partial pressure).[52] Therefore, we conclude that the photocurrent in this system is

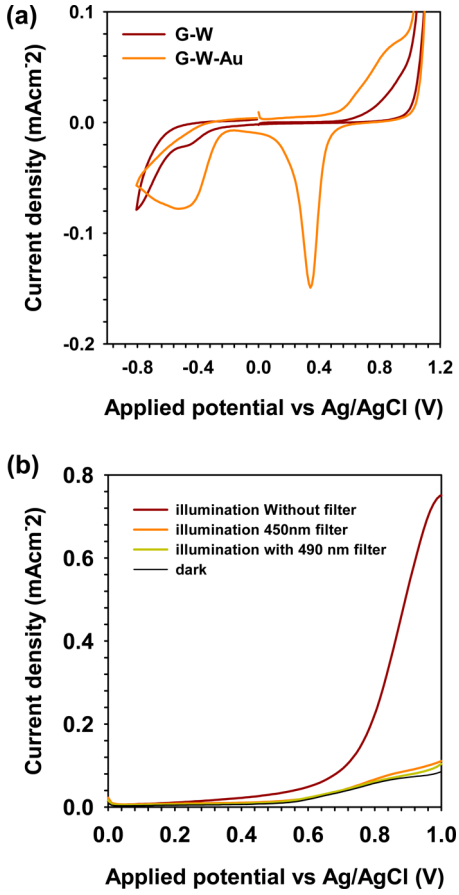


**Figure 7.** (a) Cyclic voltammograms of graphene−$WO_3$ membrane and graphene−$WO_3$−Au hybrid membrane. (b) Photoelectrochemical (PEC) *J*−*V* measurement of graphene−$WO_3$−Au electrode at different light illumination conditions. The high-pressure Xe arc lamp ((HAYASHI Co. Ltd , Japan) light source with light illumination intensity of 75 mW $cm^{-2}$ was applied for photoillumination. The 0.5M $Na_2SO_4$ and Pt foil is used for electrolyte and counter electrode, respectively, in a three-electrode PEC cell setup.

originated predominantly from $WO_3$ NPs; whereas, the AuNPs were actively facilitating the charge separation at graphene−$WO_3$−Au hybrid membrane through forming Schottky junction at electrode/electrolyte interfaces.[32] Recent reports on Au/$TiO_2$ interfaces indicate the efficient charge separation at $TiO_2$/electrolyte interfaces by plasmonic Au particle decoration.[53,54]

For the purpose of checking the activity of glucose oxidase enzyme (GOD) in this system, the electrodes were immobilized with an additional layer of GOD enzymes and their respective photocurrents were measured in presence of 0.25 mM glucose (Figure 8). It is found that the presence of GOD increases the photocurrent further due to the high sensitivity of GOD towards the oxidation of glucose. Specifically, the electrode modified with graphene-$WO_3$−Au-GOD hybrid membrane showed the maximum photocurrent generation under the same conditions. The applied potential is an important factor that is relevant to the photocurrent response in enzyme modified electrodes. Thus, it is critical to determine the optimal applied potential to fetch the maximal enzyme functionality. Figure 9 illustrates that the photocurrent generated at graphene-$WO_3$-GOD hybrid membrane modified electrode strongly depends on the applied potential. The photocurrent increases with the applied potential and reaches a

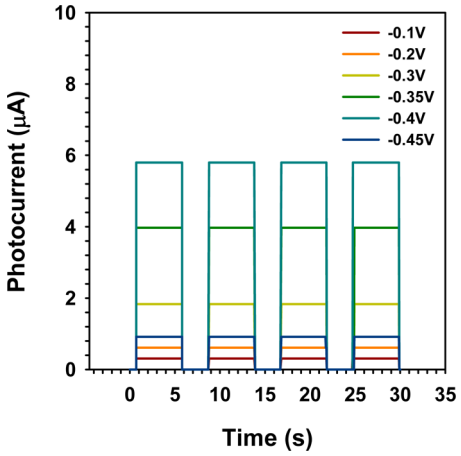


**Figure 8.** Photocurrent generated at graphene–$WO_3$ membrane decorated with GOD enzyme at various applied potentials. 0.1 M PBS buffer solution (pH 7.3) was used as supporting electrolyte.

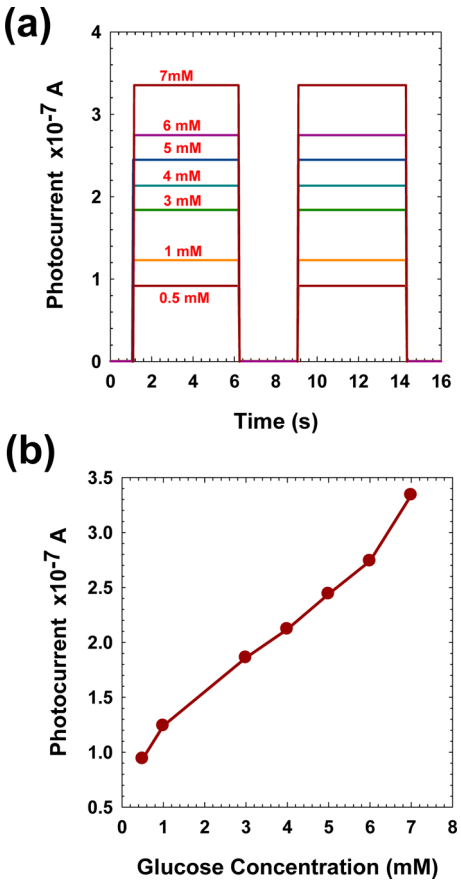


**Figure 9.** (a) Photocurrent generated at graphene–$WO_3$–Au–GOD hybrid membrane in presence of different amounts of glucose, and (b) the calibration curve of photocurrent vs glucose concentration.

maximum at −0.4 V vs. Ag/AgCl, after which the potential starts dropping down. This potential is close to the formal potential of the FAD/$FADH_2$ redox couple in GOD, indicating the direct electron transfer between the GOD and electrode.[55,56] Therefore, the optimal potential of -0.4 V vs. Ag/AgCl was selected for the photocurrent measurements. Owing to the high stability of the enzyme at neutral pH, 0.1 M PBS buffer (pH 7.3) was used as the supporting electrolyte in all photo-electrochemical measurements.

To analyze the photo-electrochemical sensing ability of the modified electrodes, we measured the photocurrent generated from various electrodes at different glucose concentration. Under optimal conditions, Figure 9a depicts the typical time-based photocurrent response of photo-electrochemical biosensor formed using graphene–$WO_3$–Au–GOD hybrid membrane in the presence of different concentration of glucose. The cathodic peak current is proportional to the concentration of the glucose, which results from the consumption of dissolved $O_2$. The typical mechanism of the reaction at the cathode in presence of GOD enzyme can be explained as follows

$$\text{glucose} + O_2 \rightarrow \text{gluconic acid} + H_2O_2 \quad (1)$$

Thus the presence of GOD enzyme readily oxidises the glucose and hence supplies electrons to the electrode. Figure 9b shows the linear dependence of the photocurrent with that of the glucose concentration. Figure S6 in the Supporting Information shows the calibration curves obtained from the response of various electrodes to different concentration of glucose. It is observed from the calibration curve that the electrodes modified with graphene–$WO_3$ membranes show a linear increase in photocurrent with the addition of glucose. However, after a certain concentration of glucose, 0.15 mM, the photocurrent reaches saturation. Although the graphene–$WO_3$–Au hybrid membrane and graphene–$WO_3$–GOD membranes show higher photocurrent generations than graphene–$WO_3$ membranes for the same glucose concentration, the photocurrent reaches the saturation at about 0.25 mM of glucose, respectively. In striking contrast, graphene–$WO_3$–Au–GOD hybrid membrane modified electrodes shows a wide linear range with the concentration of the glucose from 0.5 mM to 7 mM glucose, which shows the larger detection range together with the enhanced photocurrent generation. This could be ascribed to the synergistic effects of GOD enzyme and AuNPs. It is worth mentioning that the pristine graphene showed higher degree of instability under similar conditions. However, the evenly dispersed $WO_3$ nanoparticles protect the graphene contact with aqueous electrolyte and thus improving the durability of graphene. The work function of $WO_3$ situated ~0.4 eV above the Fermi level of graphene (see the Supporting Information, S2) affords favorable electronic interfaces for photoelectron injection from $WO_3$ to the graphene matrix. In addition, the highly interconnected underneath graphene layer facilitates the high charge collection from the $WO_3$ layer to the external circuit. Furthermore, the photoelectrochemical measurements corroborate that the AuNPs play a dual role of improving the catalytic activity of the immobilized enzyme as well as promote the charge separation at electrode/electrolyte interfaces. Thus, our proposed electrode architecture of unique triplet junction structure synergistically contributes to the enhanced photocurrent generation and thus increased sensing performance. It is anticipated that visible-light-activated graphene–$WO_3$–Au photoelectrodes can be readily used for other promising photoelectrochemical cells, including PEC water splitting hydrogen generation.

## 4. CONCLUSIONS

In summary, the present work focuses on the fabrication of graphene–$WO_3$ membranes as a potential alternative photoanode in photoelectrochemical glucose sensing applications and the possibility of fortifying its photocatalytic activity using

plasmonic gold nanoparticles. The photoelectrochemical tests show that the performance of AuNPs supported on graphene–$WO_3$ membrane is superior to other systems those without backbone conducting channel. Although more detailed investigations are needed to improve their selectivity for glucose sensing, our reported results would substantially improve the application of $WO_3$-based electrodes as an alternative to $TiO_2$ nanomaterials in photoelectrochemical-based applications.

## ■ ASSOCIATED CONTENT

### Supporting Information

Detail of experimental scheme, UPS, AFM, TEM, EDS results, and glucose sensitivity data. This material is available free of charge via the Internet at http://pubs.acs.org.

## ■ AUTHOR INFORMATION


### Corresponding Authors

*E-mail: upaik@hanyang.ac.kr.
*E-mail: Wonbong.Choi@unt.edu

### Author Contributions

†Authors A.D. and P.S. contributed equally.


### Notes

The authors declare no competing financial interest.

## ■ ACKNOWLEDGMENTS

This work was supported by the Global Research Laboratory (GRL) Program (K20704000003TA050000310) through the National Research Foundation of Korea (NRF) funded by the Ministry of Science, ICT (Information and Communication Technologies) and Future Planning, an International Cooperation program of the Korea Institute of Energy Technology Evaluation and Planning (KETEP) grant funded by the Korean Ministry of Trade, Industry & Energy (2011T100100369), the Nano-Material Technology Development Program (2012035286) through the NRF funded by the Ministry of Science, ICT and Future Planning. This research was also supported by the Korea Center for Artificial Photosynthesis (KCAP, NRF-2012-M1A2A2671834), the Priority Research Centers Program (2011-0031407). P.S. acknowledges the financial support from Japan Society for the Promotion of Science (JSPS) for providing a Postdoctoral Research Fellowship.

## ■ REFERENCES


(1) Fujishima, A.; Honda, K. Electrochemical Photolysis of Water at a Semiconductor Electrode. *Nature* **1972**, *238*, 37–38.

(2) Rodenas, P.; Song, T.; Sudhagar, P.; Marzari, G.; Han, H.; Badia-Bou, L.; Gimenez, S.; Fabregat-Santiago, F.; Mora-Sero, I.; Bisquert, J.; Paik, U.; Kang, Y. S. Quantum Dot Based Heterostructures for Unassisted Photoelectrochemical Hydrogen Generation. *Adv. Energy Mater.* **2013**, *3*, 176–182.

(3) Sudhagar, P.; Asokan, K.; Ito, E.; Kang, Y. S. N-Ion-implanted $TiO_2$ Photoanodes in Quantum Dot-sensitized Solar Cells. *Nanoscale* **2012**, *4*, 2416–2422.

(4) Uddin, M. T.; Nicolas, Y.; Olivier, C.; Toupance, T.; Servant, L.; Müller, M. M.; Kleebe, H.-J.; Ziegler, J.; Jaegermann, W. Nanostructured $SnO_2$–ZnO Heterojunction Photocatalysts Showing Enhanced Photocatalytic Activity for the Degradation of Organic Dyes. *Inorg. Chem.* **2012**, *51*, 7764–7773.

(5) Yue, Z.; Lisdat, F.; Parak, W. J.; Hickey, S. G.; Tu, L.; Sabir, N.; Dorfs, D.; Bigall, N. C. Quantum-Dot-Based Photoelectrochemical Sensors for Chemical and Biological Detection. *ACS Appl. Mater. Interfaces* **2013**, *5*, 2800–2814.

(6) Tokudome, H.; Yamada, Y.; Sonezaki, S.; Ishikawa, H.; Bekki, M.; Kanehira, K.; Miyauchi, M. Photoelectrochemical Deoxyribonucleic Acid Sensing on a Nanostructured $TiO_2$ Electrode. *Appl. Phys. Lett.* **2005**, *87*, 213901.

(7) Lightcap, I. V.; Kamat, P. V. Fortification of CdSe Quantum Dots with Graphene Oxide. Excited State Interactions and Light Energy Conversion. *J. Am. Chem. Soc.* **2012**, *134*, 7109–7116.

(8) Wang, G.-L.; Xu, J.-J.; Chen, H.-Y. Dopamine Sensitized Nanoporous $TiO_2$ Film on Electrodes: Photoelectrochemical Sensing of NADH Under Visible Irradiation. *Biosens. Bioelectron.* **2009**, *24*, 2494–2498.

(9) Wang, K.; Wu, J.; Liu, Q.; Jin, Y.; Yan, J.; Cai, J. Ultrasensitive Photoelectrochemical Sensing of Nicotinamide Adenine Dinucleotide Based on Graphene-$TiO_2$ Nanohybrids Under Visible Irradiation. *Analytica Chimica Acta* **2012**, *745*, 131–136.

(10) Hu, Y.; Xue, Z.; He, H.; Ai, R.; Liu, X.; Lu, X. Photoelectrochemical Sensing for Hydroquinone Based on Porphyrin-functionalized Au Nanoparticles on Graphene. *Biosens. Bioelectron.* **2013**, *47*, 45–49.

(11) Zheng, M.; Cui, Y.; Li, X.; Liu, S.; Tang, Z. Photoelectrochemical Sensing of Glucose Based on Quantum Dot and Enzyme Nanocomposites. *J. Electroanal. Chem.* **2011**, *656*, 167–173.

(12) Kang, Q.; Yang, L.; Chen, Y.; Luo, S.; Wen, L.; Cai, Q.; Yao, S. Photoelectrochemical Detection of Pentachlorophenol with a Multiple Hybrid $CdSe_xTe_{1-x}/TiO_2$ Nanotube Structure-Based Label-Free Immunosensor. *Anal. Chem.* **2010**, *82*, 9749–9754.

(13) Cross, W. B.; Parkin, I. P. Aerosol Assisted Chemical Vapour Deposition of Tungsten Oxide Films From Polyoxotungstate Precursors: Active Photocatalysts. *Chem. Commun.* **2003**, *0*, 1696–1697.

(14) Santato, C.; Ulmann, M.; Augustynski, J. Photoelectrochemical Properties of Nanostructured Tungsten Trioxide Films. *J. Phys. Chem. B* **2001**, *105*, 936–940.

(15) Su, J.; Guo, L.; Bao, N.; Grimes, C. A. Nanostructured $WO_3$/$BiVO_4$ Heterojunction Films for Efficient Photoelectrochemical Water Splitting. *Nano Lett.* **2011**, *11*, 1928–1933.

(16) Liu, G.; Niu, P.; Sun, C.; Smith, S. C.; Chen, Z.; Lu, G. Q.; Cheng, H.-M. Unique Electronic Structure Induced High Photoreactivity of Sulfur-Doped Graphitic $C_3N_4$. *J. Am. Chem. Soc.* **2010**, *132*, 11642–11648.

(17) Youngblood, W. J.; Lee, S.-H. A.; Maeda, K.; Mallouk, T. E. Visible Light Water Splitting Using Dye-Sensitized Oxide Semiconductors. *Acc. Chem. Res.* **2009**, *42*, 1966–1973.

(18) Zhou, W.; Yin, Z.; Du, Y.; Huang, X.; Zeng, Z.; Fan, Z.; Liu, H.; Wang, J.; Zhang, H. Synthesis of Few-Layer $MoS_2$ Nanosheet-Coated $TiO_2$ Nanobelt Heterostructures for Enhanced Photocatalytic Activities. *Small* **2013**, *9*, 140–147.

(19) Han, H.; Sudhagar, P.; Song, T.; Jeon, Y.; Mora-Sero, I.; Fabregat-Santiago, F.; Bisquert, J.; Kang, Y. S.; Paik, U. Three Dimensional-$TiO_2$ Nanotube Array Photoanode Architectures Assembled on a Thin Hollow Nanofibrous Backbone and Their Performance in Quantum Dot-Sensitized Solar Cells. *Chem. Commun.* **2013**, *49*, 2810–2812.

(20) Xiang, Q.; Yu, J.; Jaroniec, M. Graphene-based Semiconductor Photocatalysts. *Chem. Soc. Rev.* **2012**, *4*, 782–796.

(21) Zhang, H.; Lv, X.; Li, Y.; Wang, Y.; Li, J. P25-Graphene Composite as a High Performance Photocatalyst. *ACS Nano* **2009**, *4*, 380–386.

(22) Wang, P.; Huang, B.; Dai, Y.; Whangbo, M.-H. Plasmonic Photocatalysts: Harvesting Visible Light with Noble Metal Nanoparticles. *Phys. Chem. Chem. Phys.* **2012**, *14*, 9813–9825.

(23) Zhang, N.; Zhang, Y.; Xu, Y.-J. Recent Progress on Graphene-based Photocatalysts: Current Status and Future Perspectives. *Nanoscale* **2012**, *4*, 5792–5813.

(24) Ng, Y. H.; Iwase, A.; Kudo, A.; Amal, R. Reducing Graphene Oxide on a Visible-Light BiVO4 Photocatalyst for an Enhanced Photoelectrochemical Water Splitting. *J. Phys. Chem. Lett.* **2010**, *1*, 2607–2612.

(25) Krishnamoorthy, K.; Veerapandian, M.; Yun, K.; Kim, S. J. The Chemical and Structural Analysis of Graphene Oxide with Different Degrees of Oxidation. *Carbon* **2013**, *53*, 38−49.
(26) Das, S.; Sudhagar, P.; Kang, Y. S.; Choi, W. Graphene Synthesis and Application for Solar Cells. *J. Mater. Res.* **2014**, *29*, 299−319.
(27) Waterhouse, M. M.; Nadeem, G. I. N.; Metson, M. A.; Keane, J. B.; Howe, M. A.; LlorcaJ, R. F.; IdrissH. The Effect of Gold Loading and Particle size on Photocatalytic Hydrogen Production From Ethanol Over Au/$TiO_2$ Nanoparticles. *Nat. Chem.* **2011**, *3*, 489−492.
(28) Devadoss, A.; Dickinson, C.; Keyes, T. E.; Forster, R. J. Electrochemiluminescent Metallopolymer−Nanoparticle Composites: Nanoparticle Size Effects. *Anal. Chem.* **2011**, *83*, 2383−2387.
(29) Hou, W.; Cronin, S. B. A Review of Surface Plasmon Resonance-Enhanced Photocatalysis. *Adv. Funct. Mater.* **2013**, *23*, 1612−1619.
(30) Chen, H. M.; Chen, C. K.; Chen, C.-J.; Cheng, L.-C.; Wu, P. C.; Cheng, B. H.; Ho, Y. Z.; Tseng, M. L.; Hsu, Y.-Y.; Chan, T.-S.; Lee, J.-F.; Liu, R.-S.; Tsai, D. P. Plasmon Inducing Effects for Enhanced Photoelectrochemical Water Splitting: X-ray Absorption Approach to Electronic Structures. *ACS Nano* **2012**, *6*, 7362−7372.
(31) Zhang, X.; Chen, Y. L.; Liu, R. S.; Tsai, D. P. Plasmonic Photocatalysis. *Rep. Prog. Phys.* **2013**, *76*, 046401−046442.
(32) Xiang, Q.; Meng, G. F.; Zhao, H. B.; Zhang, Y.; Li, H.; Ma, W. J.; Xu, J. Q. Au Nanoparticle Modified WO3 Nanorods with Their Enhanced Properties for Photocatalysis and Gas Sensing. *J. Phys. Chem. C* **2010**, *114*, 2049−2055.
(33) Guai, G. H.; Song, Q. L.; Guo, C. X.; Lu, Z. S.; Chen, T.; Ng, C. M.; Li, C. M. Graphene Counter Electrode to Significantly Reduce Pt Loading and Enhance Charge Transfer for High Performance Dye-Sensitized Solar Cell. *Sol. Energy* **2012**, *86*, 2041−2048.
(34) Das, S.; Sudhagar, P.; Nagarajan, S.; Ito, E.; Lee, S. Y.; Kang, Y. S.; Choi, W. Synthesis of Graphene-CoS Electro-catalytic Electrodes for Dye sensitized Solar Cells. *Carbon* **2012**, *50*, 4815−4821.
(35) Veerapandian, M.; Seo, Y. T.; Shin, H.; Yun, K.; Lee, M. H. Functionalized Graphene Oxide for Clinical Glucose Biosensing in Urine and Serum Samples. *Int. J. Nanomed.* **2012**, *7*, 6123−6136.
(36) Veerapandian, M.; Kim, H. Y.; Seo, Y.-T.; Lee, K.-N.; Yun, K.; Lee, M.-H. Metalloid Polymer Nanoparticle Functionalized Graphene Oxide Working Electrode for Durable Glucose Sensing. *Mater. Res. Bull.* **2014**, *49*, 593−600.
(37) Heller, A.; Feldman, B. Electrochemistry in Diabetes Management. *Acc. Chem. Res.* **2010**, *43*, 963−973.
(38) Zhang, M.; Yu, P.; Mao, L. Rational Design of Surface/Interface Chemistry for Quantitative in Vivo Monitoring of Brain Chemistry. *Acc. Chem. Res.* **2012**, *45*, 533−543.
(39) Weinhardt, L.; Blum, M.; Bar, M.; Heske, C.; Cole, B.; Marsen, B.; Miller, E. L. Electronic Surface Level Positions of $WO_3$ Thin Films for Photoelectrochemical Hydrogen Production. *J. Phys. Chem. C* **2008**, *112*, 3078−3082.
(40) Devadoss, A.; Han, H.; Song, T.; Kim, Y.-P.; Paik, U. Gold Nanoparticle-composite Nanofibers for Enzymatic Electrochemical Sensing of Hydrogen Peroxide. *Analyst* **2013**, *138*, 5025−5030.
(41) Das, S.; Sudhagar, P.; Verma, V.; Song, D.; Ito, E.; Lee, S. Y.; Kang, Y. S.; Choi, W. Amplifying Charge-Transfer Characteristics of Graphene for Triiodide Reduction in Dye-Sensitized Solar Cells. *Adv. Funct. Mater.* **2011**, *21*, 3729−3736.
(42) Devadoss, A.; Dennany, L.; Dickinson, C.; Keyes, T. E.; Forster, R. J. Highly Sensitive Detection of NADH Using Electrochemiluminescent Nanocomposites. *Electrochem. Commun.* **2012**, *19*, 43−45.
(43) Dresselhaus, M. S.; Jorio, A.; Hofmann, M.; Dresselhaus, G.; Saito, R. Perspectives on Carbon Nanotubes and Graphene Raman Spectroscopy. *Nano Lett.* **2010**, *10*, 751−758.
(44) Ni, Z.; Wang, Y.; Yu, T.; Shen, Z. Raman Spectroscopy and Imaging of Graphene. *Nano Res.* **2008**, *1*, 273−291.
(45) Englert, J. M.; Dotzer, C.; Yang, G.; Schmid, M.; Papp, C.; Gottfried, J. M.; Steinrück, H.-P.; Spiecker, E.; Hauke, F.; Hirsch, A. Covalent Bulk Functionalization of Graphene. *Nat. Chem.* **2011**, *3*, 279−286.
(46) Devadoss, A.; Spehar-Délèze, A.-M.; Tanner, D. A.; Bertoncello, P.; Marthi, R.; Keyes, T. E.; Forster, R. J. Enhanced Electrochemiluminescence and Charge Transport Through Films of Metallopolymer-Gold Nanoparticle Composites. *Langmuir* **2009**, *26*, 2130−2135.
(47) Gao, H.; Liu, C.; Jeong, H. E.; Yang, P. Plasmon-Enhanced Photocatalytic Activity of Iron Oxide on Gold Nanopillars. *ACS Nano* **2011**, *6*, 234−240.
(48) Cushing, S. K.; Li, J.; Meng, F.; Senty, T. R.; Suri, S.; Zhi, M.; Li, M.; Bristow, A. D.; Wu, N. Photocatalytic Activity Enhanced by Plasmonic Resonant Energy Transfer From Metal to Semiconductor. *J. Am. Chem. Soc.* **2012**, *134*, 15033−15041.
(49) Jiangtian, L.; Scott, K. C.; Peng, Z.; Fanke, M.; Deryn, C.; Nianqiang, W., Plasmon-Induced Photonic and Energy-transfer Enhancement of Solar Water Splitting by a Hematite Nanorod Array. *Nature Communications* **2013**,*4*.
(50) Tian, Y.; Shi, X.; Lu, C.; Wang, X.; Wang, S. Charge Separation in Solid-state Gold Nanoparticles-sensitized Photovoltaic Cell. *Electrochem. Commun.* **2009**, *11*, 1603−1605.
(51) Bora, T.; Kyaw, H. H.; Sarkar, S.; Pal, S. K.; Dutta, J. Highly efficient ZnO/Au Schottky Barrier Dye-sensitized Solar cells: Role of Gold Nanoparticles on the Charge-transfer Process. *Beilstein J. Nanotechnol.* **2011**, *2*, 681−690.
(52) Vemuri, R. S.; Engelhard, M. H.; Ramana, C. V. Correlation Between Surface Chemistry, Density, and Band Gap in Nanocrystalline $WO_3$ Thin Films. *ACS Appl. Mater. Interfaces* **2012**, *4*, 1371−1377.
(53) Du, L.; Furube, A.; Yamamoto, K.; Hara, K.; Katoh, R.; Tachiya, M. Plasmon-Induced Charge Separation and Recombination Dynamics in Gold−$TiO_2$ Nanoparticle Systems: Dependence on TiO2 Particle Size. *J. Phys. Chem. C* **2009**, *113*, 6454−6462.
(54) Bian, Z.; Tachikawa, T.; Zhang, P.; Fujitsuka, M.; Majima, T. Au/$TiO_2$ Superstructure-Based Plasmonic Photocatalysts Exhibiting Efficient Charge Separation and Unprecedented Activity. *J. Am. Chem. Soc.* **2013**, *136*, 458−465.
(55) Wang, D.; Chen, L. Facile Direct Electron Transfer in Glucose Oxidase Modified Electrodes. *Electrochim. Acta* **2009**, *54*, 4316−4320.
(56) Kang, X.; Wang, J.; Wu, H.; Aksay, I. A.; Liu, J.; Lin, Y. Glucose Oxidase−Graphene−Chitosan Modified Electrode for Direct Electrochemistry and Glucose Sensing. *Biosens. Bioelectron.* **2009**, *25*, 901−905.